Cathodoluminescence microscopy: Optical imaging and spectroscopy with deep-subwavelength resolution

Toon Coenen, Benjamin J.M. Brenny, Ernst Jan Vesseur, and Albert Polman

Center for Nanophotonics, FOM Institute AMOLF

Science Park 104, 1098 XG, Amsterdam, the Netherlands

Email: polman@amolf.nl

Abstract

We describe a new microscope, based on angle-resolved cathodoluminescence imaging spectroscopy, that enables optical imaging and spectroscopy at deep-subwavelength spatial resolution. We use a free electron beam in a scanning electron microscope as a direct excitation source of polarizable material and collect the emitted coherent visible/infrared cathodoluminescence radiation using a specially designed optical collection system that is integrated in the electron microscope. We demonstrate the use of this new technique for the excitation of plasmons in single metal nanoparticles, surface plasmon polaritons at metal surfaces, resonant Mie modes in dielectric nanostructures and cavity modes and Bloch modes in photonic crystals. Using angle-resolved detection we are able to derive the nature of localized modes and the dispersion of propagation modes in dielectric and plasmonic geometries. An outlook is provided of new directions and applications of cathodoluminescence imaging spectroscopy.

1. Introduction

With the growing importance of nanotechnology the demand for high-resolution microscopy and characterization techniques has strongly increased. Conventional optical microscopy is limited in resolution by the diffraction limit for light, making it unsuited for optical studies at the nanoscale. Near-field optical microscopy,[1] in which a nanoscale tip scans over a surface to collect radiation provides higher spatial resolution, but is experimentally complex and often suffers from unavoidable interaction between the tip and the analyzed surface. Other advanced microscopy techniques such as stimulated emission depletion microscopy (STED),[2] photoactivated localization microscopy (PALM)[3] and stochastic optical reconstruction microscopy (STORM),[4] for example, show subwavelength resolution, but require the use of fluorescent labels. A label-free optical imaging technique with deep-subwavelength resolution that has recently gained significant interest is based on the use of a focused beam of fast electrons as an optical excitation source. As electrons can be focused to nanoscale dimensions, this technique shows deep-subwavelength optical resolution.

Fundamentally, an electron beam is a very pure optical excitation source. The time-varying evanescent electric field around the electron trajectory can interact with a polarizable medium, resulting in elemental optical materials excitations. These excitations can be probed by studying the energy loss of the electrons (Electron Energy Loss Spectroscopy, EELS) or by detecting the optical radiation that is subsequently emitted by the material (cathodoluminescence, CL).[5] The spatial resolution of excitation is determined by the electron beam spot size, which is on the order of a nanometer, as well as the radial extent of the evanescent electric field about the electron beam, which is of order 10 nm, depending on the beam energy. The spectral extent of the excitation is determined by the interaction time of the electron with the sample which is typically less than 1 femtosecond. This is less than one optical cycle of the emitted radiation and thus corresponds to a broad spectral range, making the moving electron a broadband optical excitation source spanning the UV/visible/infrared spectral range.

Electron beams can also excite materials by impact excitation or through secondary electrons generated inside the material. This incoherent CL emission has been known for many decades and is used in the study of optically active semiconductors, quantum dots, lanthanide ions, and radiative point defects in materials. As the secondary electron cloud is much larger in size than the primary electron beam, the spatial resolution of incoherent CL imaging is usually poor, except when confocal light collection techniques are used,[6] in which case the resolution is limited by the diffraction limit.

This article focuses on the coherent excitation method offered by electron beam excitation in which the electron beam is used as a direct excitation source for characteristic materials resonances in nanostructured optical materials. This excitation mechanism can usually be purely described by

electrodynamics, and requires knowledge of only the electron beam energy, materials geometry, and materials optical constants.[1,7] In this article we will review a new microscope that we have designed and built to utilize this deep-subwavelength excitation method, and will highlight some of the fundamental nanophotonics insights that we have gained with it.

2. Cathodoluminescence imaging instrument

The main component of the new instrument is a 30 keV scanning electron microscope (SEM, FEI XL-30) equipped with Schottky field emission gun (see Figure 1a). This electron source provides the nA beam currents that are required to obtain sufficient CL signal. The SEM is equipped with a specially designed micromanipulation stage that carries an off-axis aluminum paraboloid mirror with a 1.46π sr acceptance angle (Figure 1b,c). The electron beam reaches the sample through a 600-µm-diameter hole in the paraboloid, directly above its focal point. The mirror collects the generated CL and redirects it out of the SEM through a glass vacuum flange into an enclosed optics box (black box in Figure 1a). The micromanipulation stage allows for proper focusing of the paraboloid by using four piezoelectric stepper motors connected to a titanium leaf spring system (visible in Figure 1b). This system provides translational degrees of freedom (*x*,*y*) as well as control over mirror tilt and yaw. Vertical alignment of the sample with the mirror focus is achieved by varying the SEM stage height. Achieving precise alignment of the parabola's focus and beam path with the nanostructure under investigation is essential to collect reproducible and well-calibrated CL data.

Figure 1d shows a schematic of the CL setup. For spectral imaging purposes, the CL that is collected by the paraboloid is focused onto a multimode fiber using an achromatic lens. The fiber is connected to one of two spectrometers, with either a liquid-nitrogen-cooled silicon CCD array (sensitivity wavelength range λ = 400 - 900 nm) or a liquid-nitrogen-cooled InGaAs photodiode array (λ = 900 - 1650 nm). In CL imaging mode, the electron beam is raster-scanned over the surface and a spectrum is taken at every beam position. In this way a three-dimensional CL intensity datacube with *x*-position/*y*-position/wavelength coordinates is collected. A typical two-dimensional spatial scan composed of 50x50 pixels in *x* and *y* direction is taken in 10 minutes. To avoid the effect of beam drift during CL measurements, SEM images are recorded regularly during the measurements and the measurement area is adjusted if needed. Indeed, CL imaging is a powerful correlative technique in which SEM and CL images can be directly overlaid and compared.

A second important feature of the CL instrument is the capability to measure the angular distribution of the emitted radiation.[8,9] The 2D lateral intensity profile of the parallel beam emanating from the paraboloid mirror is a direct measure of the angular emission distribution. We measure the beam profile by directing it to a two-dimensional Peltier-cooled back-illuminated 1024x1024 pixel CCD array. A schematic illustration of this type of measurement is shown in Figure 1e. The achromatic

lens is defocused to ensure that the beam fills the entire CCD array. This collection geometry is similar to “Fourier imaging”, also known as “conoscopic imaging”, or “defocused imaging” in microscopy: the wave vector distribution of emitted light is directly imaged onto the CCD. If the mirror is well-focused, each point in the CCD image corresponds to light reflected off a single point on the paraboloid and thus corresponds to a unique emission angle described by a zenithal angle θ running from 0° to 90° (where θ = 0° is normal to the surface) and azimuthal angle ϕ running from 0° to 360° (where the paraboloid vertex is at ϕ = 180°). Using the proper coordinate transform, the data collected on the CCD are converted to units of emitted power per steradian. To obtain spectral selectivity in this angle-resolved measuring mode, 40-nm-band-pass color filters are used. A typical wavelength-filtered angular measurement at a single beam position is taken in 30 seconds. In a second geometry, a pinhole is placed in the optical beam path and scanned in a plane normal to the emitted beam while the collected radiation is analyzed using a spectrometer. In this way, angle- and spectrally-resolved data can be taken at the same time. Such measurements provide higher spectral resolution but at the expense of a longer measuring time. Other optical components such as polarizers and retarders can also be introduced in the optical beam path.

3. Results

3.1. Incoherent versus coherent emission

Figure 2a shows a CL spectrum taken from a bulk gallium arsenide crystal measured using our CL setup. It clearly shows the characteristic band-edge emission at λ_0 = 870 nm.[10] The measured azimuthally-averaged angular emission distribution around λ_0 = 870 nm is shown in Figure 2b. A Lambertian angular profile is found, consistent with an isotropic emission distribution within the GaAs crystal (see inset in Figure 2a). The emission observed here is the “classical” incoherent cathodoluminescence observed in many systems before. Angular measurements of incoherent CL can find applications in characterization of opto-electronic devices such as e.g. light-emitting diodes and solar cells.

Next, we study the coherent emission that occurs when the incident electron beam passes through the vacuum/material interface. Figure 2c shows this “transition radiation” (TR) spectrum for a polished surface of an aluminum single crystal.[10] A broad featureless spectrum is observed over the entire spectral range collected by the detector (λ_0 = 400 - 900 nm). This TR radiation can be explained to first order by a simple electrodynamic model, in which the electron approaching the interface induces an image charge in the metal, thus inducing an effective vertical dipole moment that is oriented upward. This transient dipole then decays into the far field with a characteristic doughnut emission pattern. The observed CL spectrum clearly reflects the inherent broad spectral nature of the

electron-beam induced excitation process as discussed above. The vertical scales in Figure 2a,c indicate the absolute emission rates per incident photon, per unit bandwidth. When integrated over the spectral range shown in Figure 2c, the TR emission rate is about 2×10^{-4} photons per incident electron.

The measured angular emission pattern at λ_0 = 400 nm is shown in Figure 2d together with a calculation of the TR radiation pattern;[5] very good agreement between the two distributions is observed. The spectrum and angular profile of TR are only determined by the electron beam energy and the optical constants of the substrate. Note that aluminum, like most metals, does not exhibit efficient intraband optical transitions and hence the spectrum in Figure 2b is dominated by TR. We note that a TR band is also present in the spectrum for GaAs in Figure 2a. However, it is overshadowed by the ~5000 times stronger incoherent band gap emission. As TR is such a well-characterized phenomenon, and metals show only weak incoherent emission, we use the combination of TR measurements and calculations for either single-crystal Al or Ag to calibrate the CL system, so that absolute CL measurements can be performed on other samples.

3.2 Excitation of plasmonic nanoparticles

Next, we investigate the electron beam induced generation of nanoscale optical resonators. The inset in Figure 3a shows a SEM image of a single Au nanodisk on a Si substrate, made using electron beam lithography and liftoff techniques. The Au nanoparticle is 100 nm in diameter and has a height of 80 nm. Figure 3a shows a CL spectrum taken by spatially averaging the CL emission collected from a raster scan over the particle with 5 nm resolution. A clear resonant spectrum is observed, that reflects the radiation of a vertically-oriented dipolar plasmon resonance in the Au nanoparticle, peaking at λ_0 = 560 nm. Plasmons are elementary excitations of free electrons in metals. They can be efficiently excited as the electric field of the electron beam passing through the nanoparticle can couple to these unbound charges. The line width of the resonant peak in the spectrum is determined by radiative and Ohmic damping. A spatial map of the CL emission is also shown in Figure 3a; it shows the nanoparticle plasmon is excited for all beam positions, but most efficient in the center, where the electron beam direction aligns with the particle eigenmode's vertical dipole moment. Plasmonic metal nanoparticles and particle networks can find applications in e.g. antennas to enhance spontaneous emission,[11] building blocks in subwavelength optical integrated circuits,[12] to create optical hot spots for sensing,[13] to enhance light absorption in photodetectors[14] and thin-film solar cells,[15] photothermal therapy,[16] and as transparent conducting nanowire meshes.[17,18]

The angular distribution of the radiation emitted by the single Au nanoparticle is shown in Figure 3b, for the case in which the electron beam placed on the left edge of the nanoparticle (see cartoon in Figure 3b).[19] The CL emission intensity is shown as function of zenithal angle θ and azimuthal angle ϕ.

The black region around $\phi = 0°$ where no light is observed corresponds to the opening in the paraboloid mirror (see Figure 1b,c). While the nanoparticle excited in the center (data not shown) shows a symmetric angular profile reflecting the doughnut-type emission from an upward-pointing dipole, in this case the measured angular distribution shows a clear left-right asymmetry. CL emission is more intense towards the right side of the angular pattern (around $\phi = 90°$) than for the left side (around $\phi = 270°$). This asymmetry arises from the fact that off-center excitation with the electron beam leads to the simultaneous excitation of in-plane and out-of-plane dipole components which interfere in the far-field.[20] This nanoscale beaming effect co-rotates with the electron beam excitation position (data not shown). A more detailed analysis of the far-field interference of dipolar electric and magnetic dipole modes, as well as quadrupolar modes is given in Refs. 20,21.

3.3 Excitation of surface plasmon polaritons

Because the electron-beam induced excitation is very localized, it represents a large range of optical wave vectors. This, together with the inherently broad excitation spectrum, allows direct excitation of surface plasmon polaritons (SPPs). These guided surface waves have in-plane momenta that are larger than that of free-space light at the same frequency and thus cannot be directly excited with light. SPPs are transverse-magnetic waves, with their electric field pointing in the normal direction, and thus couple well with the incident electron beam. In a simple model, the point dipole composed of the incident electron and it image charge in the metal decays, according to Fermi's Golden Rule, to the available modes, in this case both the far field (transition radiation) and SPPs.

Figure 4a shows an SEM image of a 400-nm-deep elliptical cavity that is sculpted into the surface of a single-crystal gold crystal using focused ion beam milling.[22] These structures serve as cavities for SPPs that propagate at the Au surface and are confined within the cavity walls. The SPP cavity modes are excited with the electron beam, and CL emission is observed due to scattering of SPPs at the cavity walls into the far field. Figure 4b shows a two-dimensional spatial excitation map taken at an emission wavelength of $\lambda_0 = 720$ nm. Two hotspots are clearly observed that result from the interference of SPPs within the cavity. This modal pattern strongly depends on the size of the SPP wave compared to the cavity size. If the cavity is large compared to the wavelength higher-order modes are supported and the interference patterns become more complex.[22] An angular emission pattern of the elliptical cavity that is excited in one of the emission maxima is shown in Figure 4c. It shows clear directional beaming of light at a wavelength of $\lambda = 600$ nm.

Figure 4d shows an SEM image of a linear SPP waveguide composed of a dielectric silica core surrounded by Ag.[23] In such coaxial waveguides strong coupling occurs between SPPs that propagate at the internal silica/Ag interfaces, and a hybrid SPP mode forms of which the dispersion (the relation

between wave vector and frequency) strongly depends on the core dimensions. The silica/Ag waveguide has a length of 2 μm and therefore standing SPP waves will form due to reflection of SPPs at the waveguide outer facets. CL spectra were taken by scanning the electron beam along the central axis of the waveguide (dashed line in Figure 4c).

Figure 4e shows these standing waves, taken at a broad range of emission wavelengths in the range λ_0 = 500 - 1000 nm. At each collection wavelength, or vacuum optical frequency, a characteristic standing wave pattern is observed of which the period is determined by the SPP wavelength at that frequency. As can be seen, SPPs have very short wavelengths at frequencies corresponding to a free space wavelength of λ_0 = 500 nm, and long wavelengths for frequencies corresponding to a wavelength of λ_0 = 1000 nm. In this way, the SPP dispersion diagram can be fully reconstructed. In this experiment, light is mostly collected from the two output facets. As the SPPs are coherently excited there is a well-defined phase relation between these radiating point sources, which leads to a fringe interference pattern in the angular radiation patterns, as can be seen in Figure 4f.[24] Nanostructures supporting surface plasmon polaritons can find applications in e.g. subwavelength optical components,[25] lasers,[26] LEDs,[27] solar cells,[28] and sensors.[29]

3.4 Excitation of dielectric nanostructures

In the previous sections we have shown that imaging and angle-resolved CL is a powerful tool for studying localized and propagating plasmon resonances in metallic nanostructures. However, the concept of coherent electron beam excitation is generally applicable to any polarizable medium including semiconductors and dielectrics. Figure 5a shows an electron micrograph of a silicon disk fabricated by electron beam lithography in combination with reactive ion etching into the top layer of a silicon-on-insulator substrate.[30] The silicon disk shown in the image has a diameter of 200 nm and a height of 100 nm and is placed on a 300-nm-thick SiO_2 layer with a thick silicon substrate underneath. These dielectric nanocavities possess Mie-type resonant modes in which the local fields are mostly confined within the Si disk. Figure 5b shows a two-dimensional excitation map for a 320-nm-diameter disk at wavelength of λ_0 = 475 nm. A radially symmetric excitation distribution is observed that reflects the resonant field distribution in the cavity. For this particular example, a minimum is observed in the center, and several subsequent maxima and minima are observed as the electron beam is moved outward. The angular emission pattern of such a structure is shown in Figure 5c and shows upward beaming of light within a relatively narrow cone. Dielectric nanostructures can find applications in e.g. microcavity lasers,[31] integrated optical components, and light scattering layers in photovoltaics.[32]

3.5 Excitation of photonic crystals

The power of the angle-resolved detection capability becomes clear further in CL studies of photonic crystals. Figure 5d shows an electron micrograph of a 200-nm-thick Si_3N_4 membrane in which a hexagonal photonic crystal is made using a combination of electron beam lithography and reactive ion etching.[33] In this particular example, a point defect cavity is created by "removing" a hole in the center. The photonic crystal is designed such that light propagation in the plane of the crystal is forbidden for a certain wavelength band (the photonic bandgap). In the cavity, however, an optical mode can exist and its field distribution can be directly probed with CL. Figure 5e shows the spatial excitation distribution of the cavity collected at the cavity resonance wavelength of λ_0 = 650 nm. A complex field distribution pattern is observed inside the cavity and reveals features at a deep-subwavelength scale. Finally, Figure 5f shows an angular emission pattern from a regular hexagonal photonic crystal (without defect cavity). The hexagonal symmetry of the photonic crystal is clearly reflected in the azimuthal emission distribution. An emission band at a particular zenithal angle is directly related to the wave vector of the mode within the photonic crystal at the corresponding frequency and therefore, such measurements can be used to derive the photonic bandstructure of the photonic crystal in great detail. Such analysis can even be performed in a spatially resolved manner, so that the two-dimensional mode profile of the each photonic band can be separately mapped. Photonic crystals can find applications in e.g. miniature lasers,[34] LEDs,[35] on-chip optical networks and memory,[36] and sensors.[37]

3.5 CL imaging resolution

To first order, the resolution of the coherent CL imaging technique is limited by the spot size of the electron beam, which is typically in the range 1 - 10 nm, depending on SEM instrument, beam current and acceleration voltage. Furthermore, the extent of the evanescent electric field about the electron trajectory will determine the spatial range over which a polarizable nanostructure is excited. By carrying out measurements of the CL intensity across a square hole made into a thin silicon membrane, we have determined the spatial resolution for 30 keV electron beam excitation to be 30 - 40 nm.[33] The field extent can be reduced by lowering the electron energy.

4. Summary and outlook

We have developed an angle-resolved cathodoluminescence imaging spectroscopy instrument that enables excitation and imaging of photonic nanostructures at deep-subwavelength-resolution. We use the electron beam as a direct excitation source of polarizable material, creating coherently emitted radiation. In this article we have briefly reviewed our earlier work in this field; more detailed information can be found in the papers that are referenced. We showed how we can separate coherent emission from incoherent emission through angle-resolved measurements. We showed that resonant plasmonic modes are excited in single metallic nanoparticles and that surface plasmon

polaritons are excited at the surface of a metal. By imaging cavity resonant field distributions, we can derive the dispersion of surface plasmon polaritons over a broad spectral range. We also showed how resonant modes in dielectric nanocavities and photonic crystal cavities can be excited, and how the dispersion of photonic crystals can be directly mapped.

Several new directions in CL imaging spectroscopy can be envisioned. First of all, extension of the detection wavelength range into the mid-infrared will enable the study of optical phenomena in a wide range of materials, including nanostructured semiconductors and dielectrics, two-dimensional materials such as graphene and boron nitride, and more. By adding time-resolved excitation capabilities, a wealth of new opportunities will emerge in dynamic studies of light in optical nanomaterials. Furthermore, it will be interesting to explore the use of angle-resolved imaging CL in other research and application fields, opto-electronic devices, lab-on-a-chip technology, pharmaceutics, integrated optics, forensics, metallurgy, biophysics, geology, materials science and metrology. Because of its very broad applicability we expect that CL spectroscopy will play an important role in many scientific developments that will appear in the coming years.

Acknowledgements

This paper reviews work carried out in collaboration with Jorik van de Groep, Felipe Bernal Arango, and Femius Koenderink (AMOLF), David Schoen and Mark Brongersma (Stanford University), Humeyra Caglayan and Nader Engheta (University of Pennsylvania), Javier García de Abajo, Martin Kuttge, Jan Renger, Niek van Hulst (ICFO, Barcelona), and Riccardo Sapienza (Imperial College). Technical support, design, and fabrication from Hans Zeijlemaker, Ilya Cerjak, Wim Brouwer, and Jan van der Linden are gratefully acknowledged. This work is part of the research program of the Foundation for Fundamental Research on Matter (FOM) which is financially supported by the Netherlands Organization for Scientific Research (NWO). It is also supported by the European Research Counsel and by NanoNextNL, a research program funded by the Dutch Ministry of Economic Affairs. Competing financial interest: AP is co-founder, shareholder, and advisor of Delmic BV, a start-up company that has brought the CL instrument discussed here on the market. A complete overview of our CL work can be found at www.erbium.nl/arcis.htm and in Ref. 38.

Inset in the paper

Workshop Electron beam spectroscopy for nanophotonics

To stimulate the further evolution of the research field of electron beam spectroscopy for nanophotonics an MRS-endorsed workshop was held in Amsterdam, from June 2-4, 2014, chaired by A. Polman and J. García de Abajo. It brought together some 60 scientists from 13 different countries. During the meeting the state-of-the-art in CL, EELS, Photoemission Electron Microscopy (PEEM), and Scanning Tunneling Microscopy (STM) were reviewed, as well as the most recent theoretical insights into electron-matter interactions. Furthermore, the prospects of novel research directions including time-resolved spectroscopies, tomography, and small-scale coherent light sources based on free electrons were discussed. The abstracts of the workshop presentations present a good overview of the state-of-the-art in this field and are available for free download at www.amolf.nl/ebsn.

References

[1] E. Betzig and J.K. Trautman, *Science* **257**, 189 (1992).

[2] T.A. Klar and S.W. Hell, *Optics Lett.* **24**, 954 (1999).

[3] E. Betzig, G.H. Patterson, R. Sougrat, O.W. Lindwasser, S. Olenych, J.S. Bonifacino, M.W. Davidson, J. Lippincott-Schwartz, and H.F. Hess, *Science* **313**, 1642 (2006).

[4] M. Rust, M. Bates, and X. Zhuang*, Nature Meth*. **3**, 793 (2006).

[5] F. J. García de Abajo, *Rev. Mod. Phys.* **82**, 209 (2010).

[6] A.C. Zonnevylle, R.F.C. van Tol, N. Liv, A.C. Narvaez, A.P.J. Effting, P. Kruit, and J.P. Hoogenboom, *J. Microsc.* **252**, 58 (2013).

[7] F. J. García de Abajo and M. Kociak, *Phys. Rev. Lett.* **100**, 106804 (2008).

[8] T. Coenen, E. J. R. Vesseur, and A. Polman, *Appl. Phys. Lett.* **99**, 143103 (2011).

[9] N. Yamamoto, S. Ohtani, and F. J. García de Abajo, *Nano Lett.* **11**, 91 (2011).

[10] B. J. M. Brenny, T. Coenen, and A. Polman, *J. Appl. Phys.* **115**, 244307 (2014).

[11] H. Mertens, J.S. Biteen, H.A. Atwater, and A. Polman, *Nano Lett.* **6**, 2622 (2006)

[12] K.C.Y. Huang, M.K. Seo, T. Sarmiento, Y. Huo, J.S. Harris and M.L. Brongersma, *Nature Photon.*, **8**, 244, (2014).

[13] L. Novotny and N. van Hulst, *Nature Photon.* **5**, 83 (2011).

[14] H.R. Stuart and D.G. Hall*, Appl. Phys. Lett.* **69**, 2327 (1996)

[15] K.R. Catchpole and A. Polman, *Appl. Phys. Lett*. **93**, 191113 (2008)

[16] C. Ayala-Orozco, C. Urban, M.W. Knight, A.S. Urban, O. Neumann, S.W. Bishnoi, S. Mukherjee, A.M. Goodman, H. Charron, T. Mitchell, M. Shea, R. Roy, S. Nanda, R. Schiff, N.J. Halas, and A. Joshi, *ACS Nano* **8***,* 6372 (2014)

[17] J. van de Groep, P. Spinelli, and A. Polman, Nano Lett. **12**, 3138 (2012)

[18] E.C. Garnett, W. Cai, J.J. Cha, F. Mahmood, S.T. Connor, M.G. Cristoforo, Y. Cui, M.D. McGehee, and M. L. Brongersma, *Nature Mater*. **11**, 241 (2012)

[19] T. Coenen, E.J.R. Vesseur, A. Polman, and A.F. Koenderink, *Nano Lett*. **11**, 3779 (2011).

[20] T. Coenen, F. Bernal Arango, A.F. Koenderink, and A. Polman, *Nature Comm.* **5**, 3250 (2014).

[21] T. Coenen and A. Polman, *ACS Nano* **8**, 7350 (2014).

[22] D.T. Schoen, T. Coenen, F.J. García de Abajo, M.L. Brongersma, and A. Polman, *Nano Lett.* **13**, 188 (2013).

[23] E.J.R. Vesseur, T. Coenen, H. Caglayan, N. Engheta, and A. Polman, *Phys. Rev. Lett.* **109**, 013902 (2013).

[24] T. Coenen, E.J.R. Vesseur, and A. Polman, *ACS Nano* **6**, 1742 (2012).

[25] E. Verhagen, M. Spasenović, A. Polman, and L. Kuipers, *Phys. Rev. Lett.* **102**, 203904 (2009).

[26] R.F. Oulton, V.J. Sorger, T. Zentgraf, R.M. Ma, C. Gladden, L. Dai, G. Bartal, and X. Zhang, *Nature* **461**, 629 (2009).

[27] K. Okamoto, I. Niki, A. Shvartser, Y. Narukawa, T. Mukai, and A. Scherer, *Nature Mater.* **3**, 601 (2004).

[28] H.A. Atwater and A. Polman, *Nature Mater.* **9,** 205 (2010).

[29] C. Wu, A.B. Khanikaev, R. Adato, N. Arju, A. A. Yanik, H. Altug, and G. Shvets, *Nature Mater.* **11**, 69 (2012).

[30] T. Coenen, J. van de Groep, and A. Polman, *ACS Nano* **7**, 1689 (2013).

[31] D.K. Armani, T.J. Kippenberg, S.M. Spillane, and K J. Vahala, *Nature* **421**, 925 (2003).

[32] P. Spinelli, M.A. Verschuuren, and A. Polman, *Nature Comm.* **3**, 692 (2012).

[33] R. Sapienza, T. Coenen, J. Renger, M. Kuttge, N.F. van Hulst, and A. Polman, *Nature Mater.* **11**, 781 (2012).

[34] O. Painter, R.K. Lee, A. Scherer, A. Yariv, J. D. OBrien, P.D. Dapkus, and I. Kim, Science **284**, 1819 (1999)

[35] J.J. Wierer Jr., A. David, and M.M. Megens, *Nature Photon.* **3**, 163 (2009).

[36] E. Kuramochi, K. Nozaki, A. Shinya, K. Takeda, T. Sato, S. Matsuo, H. Taniyama, H. Sumikura and M. Notomi, *Nature Photon.* **8**, 474 (2014).

[37] E. Chow, L. Mirkarimi, and G. Girolami, *Opt. Lett*. **29**, 1093 (2004).

[38] *Angle-resolved cathodoluminescence nanoscopy***,** Ph.D. thesis, T. Coenen, University of Amsterdam (2014).

Biographies

Toon Coenen studied chemistry and physics at Utrecht University and obtained his PhD at the FOM Institute AMOLF in Amsterdam in 2014 in the group of Albert Polman. He co-developed the CL detection system discussed in this article and used it to investigate the nanoscale optical properties of various metallic and dielectric nanostructures.

Benjamin Brenny studied chemistry and physics at Utrecht University. He is currently a PhD candidate in the group of Albert Polman investigating infrared CL spectroscopy and mapping optical band structures of complex photonic systems using CL.

Ernst Jan Vesseur obtained his PhD at the FOM Institute AMOLF in Amsterdam in 2011 in the group of Albert Polman. He co-developed the CL detection system discussed in this article. He now works at FEI Company where he continues to watch exciting developments in the electron microscopy market.

Albert Polman is scientific group leader at the FOM Institute AMOLF in Amsterdam. His research group focuses on light management in new photovoltaic materials, optical metamaterials with properties that do not exist in nature, and the development of the CL system discussed in this paper. He is professor of photonic materials for photovoltaics at the University of Amsterdam and Fellow of the MRS.

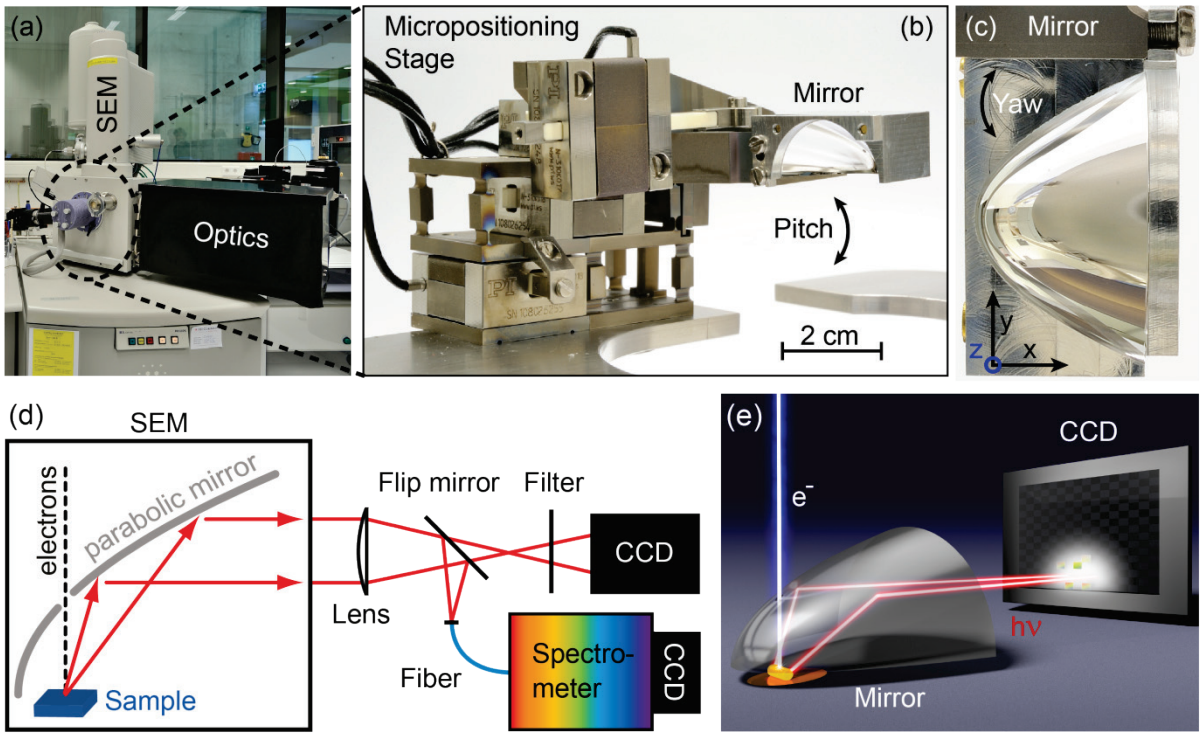

Figure 1. a Photograph of FEI XL-30 SFEG SEM with CL optics box attached. b Inside the chamber a piezoelectric mirror positioning system is mounted which is used to position a parabolic mirror in four dimensions (*x*, *y*, pitch, and yaw). c Photograph taken from the bottom of the mirror. d Schematic overview of the setup showing the different detection schemes: a spectrometer for two-dimensional CL imaging spectroscopy and a CCD imaging detector for angle-resolved measurements. e Graphical representation of angle-resolved detection of CL on a 2D CCD array (image by Tremani). Photographs in (a-c) by Henk-Jan Boluijt.

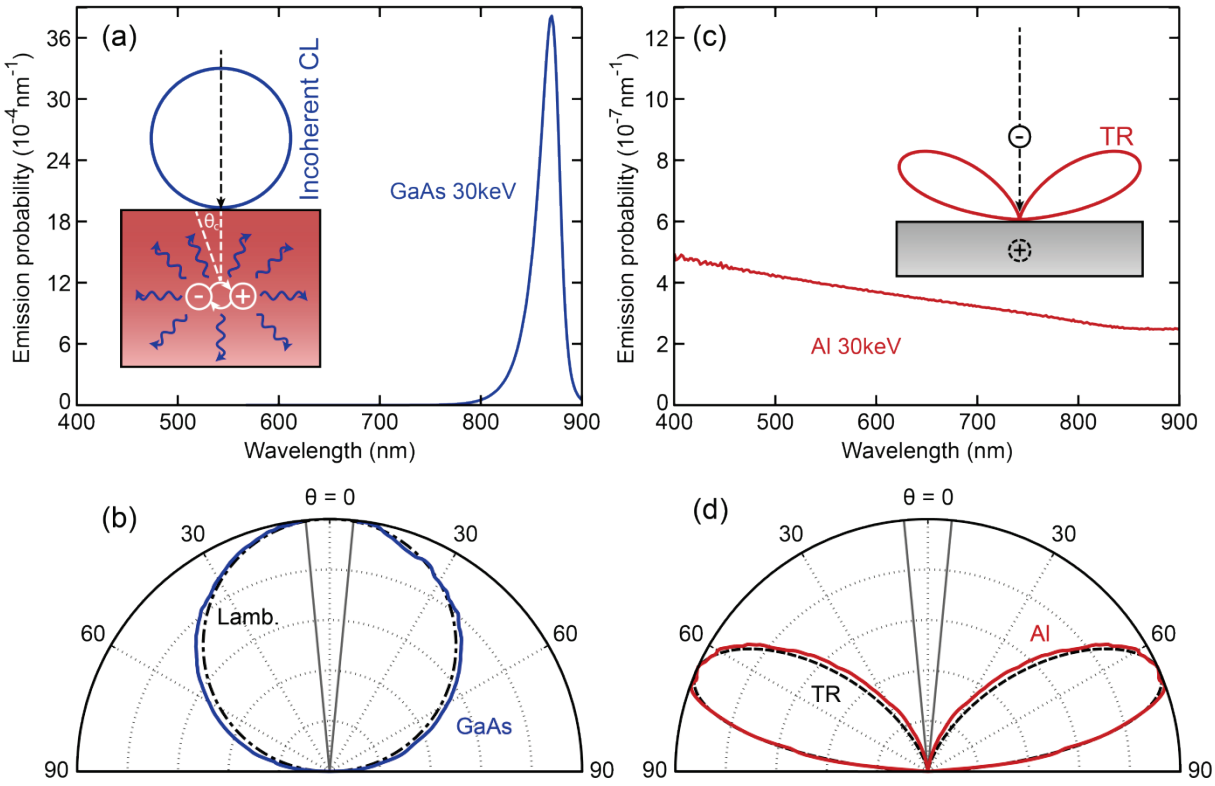

Figure 2. a Measured CL spectrum from a bulk GaAs single crystal taken at 30 keV electron energy. The inset schematically shows the isotropic radiation process inside the GaAs. Only the light within the critical angle can escape. b Measured emission pattern (blue solid line) for GaAs as function of polar angle θ (azimuthally averaged) for λ_0 = 850 nm. The black dashed line shows a theoretical Lambertian pattern. The gray solid lines indicate the angular range corresponding to the hole in the mirror, where no light is collected. c Measured CL spectrum from a bulk Al single crystal, which is dominated by transition radiation. The inset schematically indicates this process where the electron creates an image charge, giving rise to a vertical dipole at the surface which emits with a toroidal angular pattern. d Measured emission pattern (blue solid line) for Al as function of polar angle θ (azimuthally averaged) for λ_0 = 400 nm. The black dashed line shows the theoretical TR pattern. Reprinted with permission from Ref. 10, copyright 2014, American Institute of Physics.

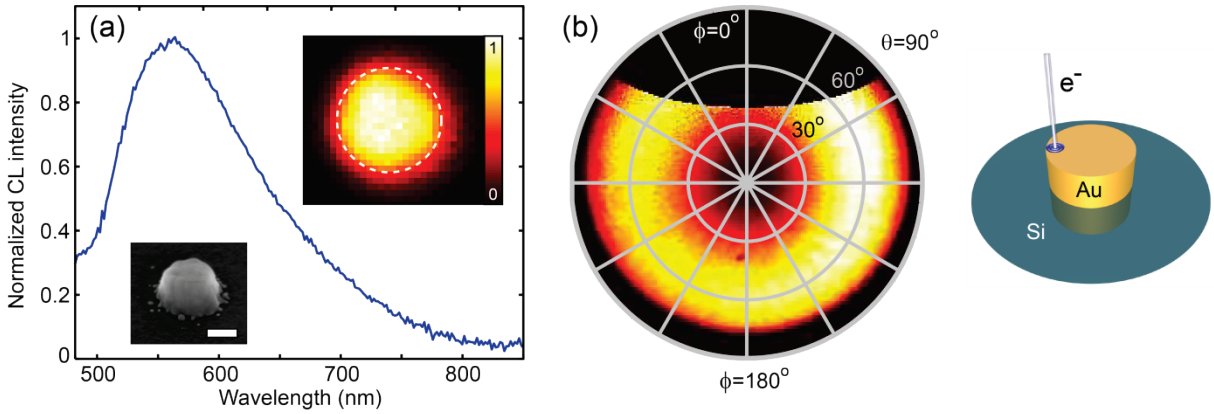

Figure 3. a Normalized CL spectrum for a Au nanodisk on Si with a diameter of 100 nm and a height of 80 nm. An SEM image is shown as an inset (scale bar: 50 nm). The spectrum is taken by averaging the CL spectrum over the particle. A two-dimensional CL excitation map taken at λ_0 = 560 nm is shown as an inset. The dashed lines indicate the edge of the structure taken from the SEM image. b Normalized CL intensity as function of azimuthal (θ) and zenithal (ϕ) angles taken at λ_0 = 600 nm for excitation on the left side of the structure. The geometry is indicated by the cartoon at the right. Reprinted with permission from Ref. 20, copyright 2014, Nature Publishing Group.

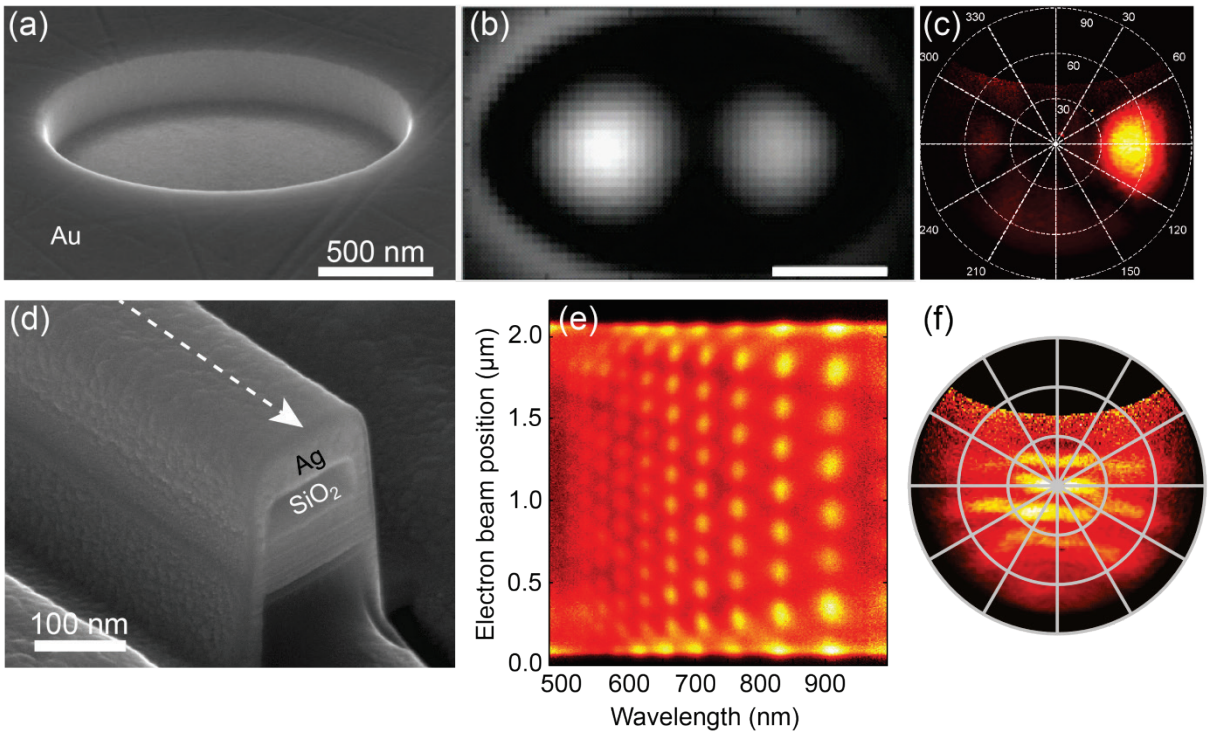

Figure 4. a SEM image of a 400-nm-deep elliptical plasmon cavity with major/minor axes of 1000/600 nm (eccentricity of 0.8) milled into a single-crystal gold substrate using FIB. b Two-dimensional CL excitation map for the ellipse in at λ_0 = 720 nm, showing a SPP resonant mode distribution. c Angular CL pattern measured on an elliptical cavity with a major/minor axes of 1500/900 nm at λ_0 = 600 nm, for excitation in the left focal spot of the ellipse. d SEM image of a 2-μm-long plasmonic waveguide with a SiO_2 core and Ag cladding. The outside of the waveguide is coated with 10 nm of Cr to suppress SPP modes on the top and bottom interfaces. e CL line scan, measured along the center of the waveguide as indicated by the white arrow in d. In this case the structure has a 400 nm wide core. f Angular CL pattern for a waveguide with a 210 nm wide core, measured at λ_0 = 700 nm for central excitation. For this measurement the waveguide was oriented from top to bottom. Reprinted with permission from Refs. 22, copyright 2013, American Chemical Society and from Ref. 23, copyright 2013, American Physical Society.

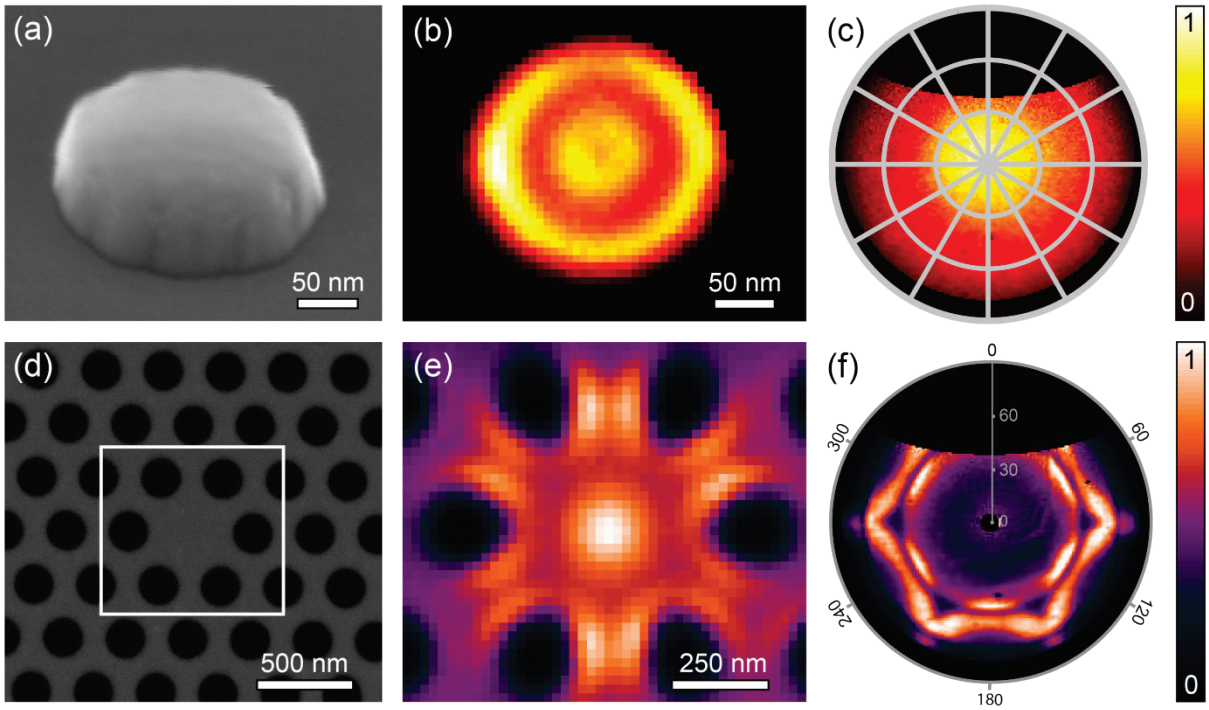

Figure 5. a SEM image of a silicon nanodisk (diameter 100 nm, height 80 nm) on a 300 nm SiO_2 layer. b 2D CL excitation map of a 320-nm-diameter silicon disk at λ_0 = 475 nm. c Angular CL pattern for a 300-nm-diameter disk collected at λ_0 = 500 nm for excitation in the center. d SEM image of a photonic crystal cavity etched in a 200-nm-thick Si_3N_4 membrane. e Two-dimensional CL excitation map of the cavity for λ_0 = 650 nm. f Angular CL pattern for the photonic crystal, taken from a regular 2D hexagonal photonic crystal, measured at λ_0 = 700 nm. Reprinted with permission from Refs. 30, copyright 2013, American Chemical Society, and from Ref. 33, copyright 2012, Nature Publishing Group.